Version 9, To be submitted to ***Chemical Physics Letters***

Entangled Biphoton Virtual-State Spectroscopy of the $A^2\Sigma^+$–$X^2\Pi$ system of OH

Jun Kojima* and Quang-Viet Nguyen

NASA Glenn Research Center
21000 Brookpark Rd, Cleveland, OH 44135, USA

*Corresponding author. Fax: (440) 962-3120, Tel: (440) 962-3095. Current address: OAI, 22800 Cedar Point Rd, Cleveland, OH 44142, USA.
E-mail address: Jun.Kojima@grc.nasa.gov, Quang-Viet.Nguyen@nasa.gov

Abstract

This Letter describes the first application of entanglement-induced virtual-state spectroscopy to a molecular system. Non-classical, non-monotonic behavior in a two-photon absorption cross section of the OH *A–X* system, induced by an entangled biphoton state is theoretically demonstrated. A Fourier transform analysis of the biphoton cross section permits access to the energy eigenvalues of intermediate rovibronic states with a fixed excitation photon energy. The dependence of the Fourier spectrum on the tuning range of the entanglement time T_e, and the relative path delay τ_e is discussed. Our analysis reveals that the implementation of molecular virtual-state spectroscopy for the OH *A–X* system requires the tuning of τ_e over a pico-second range with femto-second resolution.

The unique characteristics of entanglement-induced multi-photon spectroscopy which arise from the fourth-order quantum interference of an entangled photon with a medium (atom or molecule) have been recently discovered [1-4]. In entanglement-induced two-photon laser induced fluorescence, the fluorescence emission from the

medium being probed automatically acts as both a detector and temporal coincidence gate for the two-photon absorption process [5]. Thus, the entangled two-photon experiment would indeed display quantum interference effects in the probed medium without employing the requisite two separate detectors and coincidence circuit. The entangled two-photon absorption spectrum of atomic hydrogen was explicitly demonstrated numerically, and the resulting non-classical behavior such as a linear dependence of the two-photon absorption rate on the photon-flux density, and the non-monotonic behavior of the absorption cross section versus entanglement time were theoretically described by Fei *et al* [1]. Furthermore, a remarkable feature of this emerging spectroscopic technique was illustrated by Saleh *et al.* [2]: the ability to access intermediate states (or virtual-states) of the two-photon transition via a "transition-path-scan" without changing the wavelength of the excitation light source. In this Letter we extend this virtual-state spectroscopy to a molecular system.

The hydroxyl radical (OH) was chosen for our demonstration of entangled two-photon molecular spectroscopy because OH is one of the simplest molecules, yet is a very important species in the chemistry of many processes. The OH molecule is a key intermediate in many chemical reaction processes involving oxygen or water such as combustion or atmospheric chemistry. The spectroscopic measurement of OH provides a way to probe flame chemistry or to trace the reaction pathways in atmospheric chemistry. The use of OH in the present study has a further advantage since the molecular structure is well known, and its spectroscopy over a wide range of spectral regions has been extensively investigated [6,7]. The practical convenience of generating OH through a microwave discharge of water, or as provided from combustion products in flames is also

an important factor in an effort to implement a proof-of-concept experiment of the present technique in future.

Because of its significance, optical diagnostic techniques that probe OH have been thoroughly studied including laser absorption spectroscopy of the ground X state or laser-induced fluorescence of the A-X electronic system [6-8]. In particular, two-photon-excited fluorescence measurements have been successfully applied to the electronic system of OH [9,10] despite its very small cross section. One of the major problems in the two-photon spectroscopy of OH, is that it requires a very large excitation photon flux to gain sufficient fluorescence signals since the classical two-photon excitation occurs with randomly arriving photons (as evident by its quadratic absorption rate). Thus it suffers from a higher probability of photochemical reactions in the probe volume formed by the intense laser pulses [10,11]. This problem is significant not only for the current system but also for other kinds of classical two-photon spectroscopy, especially that as applied to the imaging of delicate biological tissues [4]. However, by using entangled biphoton pairs, the two-photon absorption rate could in theory, become comparable with that produced by classical light source but at a far lower excitation photon flux [1,4]. This arises mainly because of the *twin* photon nature of the entanglement process that produces a highly time-correlated photon pair that has a high degree of fourth-order coherence [12,13]. Thus the risk of photochemical effects can be greatly reduced. Hence, entangled biphoton spectroscopy can increase the two-photon absorption efficiency of OH, and furthermore allow us to access intermediate state information in an unprecedented way.

Absorption of an entangled photon pair. — A photon pair produced by the process of spontaneous parametric down-conversion (SPDC) within a nonlinear crystal of finite thickness, with second-order susceptibility, has the form of the twin state that is expressed as an expansion in the wave-vector space [12-14]:

$$|\mathscr{T}\rangle = \iint d\mathbf{k}_1 d\mathbf{k}_2 \Psi(\mathbf{k}_1, \mathbf{k}_2) |\mathbf{k}_1, \mathbf{k}_2\rangle \tag{1}$$

where $\mathbf{k}$ indicates the wave vector and the subscripts 1, and 2 indicate signal, and idler, respectively. $\Psi(\mathbf{k}_1, \mathbf{k}_2)$ is a nonseparable wave function in $\mathbf{k}$ space that is a function of the phase matching condition, i.e. $\mathbf{k}_1 + \mathbf{k}_2 = \mathbf{k}_p$ where p indicates pump. The entangled photons are generated via the SPDC process within an entanglement area A_e and within an entanglement time T_e [1,2], which depend on the property of the crystal and the pump.

We now consider a two-photon transition, where a quantum entangled photon pair interacts with a molecule in an initial state $|\psi_i\rangle$, with an energy eigenvalue ε_i. The photon pair excites the molecule to a final state $|\psi_f\rangle$ with energy eigenvalue ε_f through an intermediate state $|\psi_j\rangle$ with energy eigenvalue ε_j (assuming that an intermediate state linewidth can be neglected [1]). Further assuming a monochromatic pump source with the frequency $\omega_p = \varepsilon_f - \varepsilon_i$, based on second-order time-dependent perturbation theory, the entangled two-photon (or biphoton) absorption cross section may be given by [1,3]

$$\sigma_e = \frac{2\pi}{\hbar^2 \varepsilon_0^{\,2} c^2 A_e T_e} \omega_1^0 \omega_2^0 \delta(\varepsilon_f - \varepsilon_i - \omega_1^0 - \omega_2^0) \times \left| \sum_j D_j \left\{ \frac{1 - \exp\left[-iT_e \Delta_j^1\right]}{\Delta_j^1} + \frac{1 - \exp\left[-iT_e \Delta_j^2\right]}{\Delta_j^2} \right\} \right|^2 , \tag{2}$$

where $\hbar$ is the Plank constant, ε_0 is the vacuum permittivity, c is the speed of light, and $\omega_1^0 + \omega_2^0 = \omega_p$ (phase matching condition). Here, D_j represents the transition matrix

elements for the two-photon excitation process in the molecule, and is given by $D_j = \langle \psi_f | d | \psi_j \rangle \langle \psi_j | d | \psi_i \rangle$, with rovibrational or electronic transition moment d. The energy mismatch is identified as

$$\Delta_j^k = \varepsilon_j - \varepsilon_i - \omega_k^0 \ , \tag{3}$$

where the superscript $k = 1$ or 2 refers to the signal and idler photons [see Fig. 1]. The δ-function for the frequency terms ensures that energy conservation is satisfied. When the final state of the molecule is assumed to have Lorentzian broadened energy distribution with radiative lifetime (or natural lifetime), the cross section σ_e may be multiplied by the final state linewidth function and integrated over the final-state energy [2]. In this case, the δ-function removes the integral, and is simplified to become the linewidth function through the so-called sifting property. Note that the entangled two-photon absorption occurs via a *time*-entangled quantum state (twin state) given by Eq. (2) which contains T_e, a variable with time units. This entanglement time dependency does not appear in an equation describing a classical two-photon absorption process.

In order to realize virtual-state spectroscopy, another optical parameter, the relative-path-delay τ_e ($|\tau_e| < T_e$), has to be externally introduced between the two twin photons generated from the SPDC process. Based on Eq. (2) and the concept of integrating the cross section over a range of T_e, Saleh *et al* [2] derived the weighted-and-averaged entangled-photon cross section for the degenerate pump case as

$$\bar{\sigma}_e \approx \frac{\pi \omega_p^{\ 2}}{16 A_e} \delta(\varepsilon_f - \varepsilon_i - \omega_p) \bar{s}(\tau_e) \ , \tag{4}$$

where

$$\bar{s}(\tau_e) = 4\sum_{j,k} A_j A_k^* + \sum_j \left|A_j\right|^2 \left[2 + \exp(-i2\Delta_j \tau_e) + \exp(i2\Delta_j \tau_e)\right]. \quad (5)$$

Here, the coefficient $A_j = D_j / \Delta_j$. In Eq. (4) the averaging (integration) range of T_e has to be much greater than the inverse of the smallest frequency difference between neighboring intermediate states, i.e. $1/|\varepsilon_j - \varepsilon_k|$. Units here are defined as atomic units and such that $\hbar = c = 1$. As seen in Eq. (5), the relative phase of the entangled photon pair can be tuned by adjusting τ_e, and this relative-phase tuning varies the absorption amplitude. The Fourier transform of $\bar{\sigma}_e$ over a range of τ_e can then, in principle, reveal the energy mismatch terms Δ_j (in frequency space), thus the intermediate state energy as well as the transition probability term A_j (magnitude of the Fourier transform) of the molecule. The practical implementation of virtual-state spectroscopy is briefly described by Saleh *et al* [2].

Two-photon electronic transition in A-X system of OH. — To theoretically demonstrate entangled two-photon spectroscopy of OH, the $R_1(5)$ (in standard ${}^{\Delta N}\Delta J_{Ff}$ notation, with redundant labels suppressed [8,9]) rotational line of the two-photon $A^2\Sigma^+$–$X^2\Pi_i$ (0,0) transition is studied. More specifically, this is the rovibronic transition from the initial state $X^2\Pi_{3/2}$ ($v'' = 0$, $N''= 5$) to the final state $A^2\Sigma^+$ ($v' = 0$, $N'= 6$). We throughout use Hund's case (b) rotational quantum number indication (N) while the molecular structure of OH starts as case (a) at low J and switching shortly thereafter to Hund's case (b) due to the spin-orbit uncoupling. Here, the vibrational quantum number is denoted by v. The two-photon $R_1(5)$ line has been experimentally confirmed via classical two-photon fluorescence technique by Crosley and Smith [9].

The two-photon excitation of OH described above essentially involves pairs of transitions that consist of combinations of one rovibrational (infrared) transition and one rovibronic (UV) transition. Such transitions can be: 1) an X–X infrared transition followed by an A–X UV transition, or 2) an A–X UV transition followed by an A–A infrared transition. The selection rule for a two-photon electronic transition is given by $\Delta N = 0, \pm1, \pm2, \pm3$ ($\Delta J = 0, \pm1, \pm2$), which dictates the relationship between an initial state and a final state. The $R_1(5)$ line ($\Delta J = \Delta N = 1$) obeys this rule. Since a two-photon electronic transition occurs via two single-photon excitation processes, the single-photon selection rules also limit each step that is either from an initial to an intermediate state, or from an intermediate to a final state. The single-photon selection rule for an X–X transition is $\Delta N = 0, \pm1, \pm2$ ($\Delta J = 0, \pm1$). Thus only P, Q, and R branches are allowed in $^2\Pi_{3/2}$–$^2\Pi_{3/2}$ transition and ^QP, ^RQ, and ^SR branches in $^2\Pi_{1/2}$–$^2\Pi_{3/2}$ transition (hereafter the branches are given in $^{\Delta N}\Delta J$ notation for rovibrational transition, with redundant labels suppressed). As for an A–A transition, the single-photon selection rule is $\Delta J = \Delta N = \pm1$ since the total electronic orbital angular-momentum quantum number $\Lambda = 0$ for Σ state. Thus only ^PP or ^RR branches are allowed for this transition. Here satellite branches ($\Delta N = 0$) in an A–A transition is neglected because their intensities decrease rapidly (as an exponential function) with N and becomes very weak over $N = 5$. The single-photon selection rule for a A–X electronic transition is $\Delta N = 0, \pm1, \pm2$ ($\Delta J = 0, \pm1$) and there are 12 selection-rule allowed branches as described in conventional single-photon induced electronic transitions [15]. By considering the above governing selection rules, we determined five selection-rule allowed paths for the $R_1(5)$ two-photon transition that participate in the excitation process as illustrated in Fig. 2.

The rovibronic energies for OH A and X states calculated from the corresponding Hamiltonian by Luque and Crosley [7] were implemented in our simulation. The Λ–doubling and spin–orbit uncoupling effects have been incorporated into this database. The term energies they derived follow closely the data obtained by Dieke and Crosswhite [16]. A transition matrix element $\langle \psi_{v'J'}|d|\psi_{v''J''}\rangle$ for a transition from a lower state (v'', N'') to an upper state (v', N') is given by the integral of the rovibrational wavefunctions of the lower and upper states together with the transition moment. A transition moment can be either an electronic transition moment $d_e(r)$ (for an A–X) or a vibrational transition moment $d_v(r)$ (for an X–X or A–A). As for the electronic transition moment, we used the polynomial representation $d_e(r) = a_0 + a_1 \cdot r + a_2 \cdot r^2 + a_3 \cdot r^3 + \cdots$ (with internuclear distance r) following Ref. 17, and coefficients given therein. The vibrational transition moment is represented as $d_v(r) = er$ with the elementary charge e [18]. The wavefunctions (thus, the transition matrix elements) for all quantum states considered here were calculated by solving the radial Schrödinger equation using the potential energy curves for OH X and A states [19]. The potential curves were calculated by the first-order semiclassical Rydberg-Klein-Rees (RKR) method with the rotational centrifugal term [20] as shown in Fig. 1. The RKR method is a widely accepted approach for the accurate determination of potential energy functions for diatomic molecules given the vibrational and rotational term energies as input parameters [21]. In the RKR calculation, the so-called Kaiser correction, by which higher-order semiclassical effects are taken account in some level, was applied to obtain further accurate potentials for the hydrides whose reduced mass is small [20]. A steep inner wall of the potentials was smoothed over irregular or non-physical behavior by the $a \cdot e^{-br} + c$ function [20]. The v-dependences of G_v and B_v were

represented by the Dunham expression and its coefficients for OH X and A states [17]. The RKR and wavefunction calculations do not include the influence of the Λ–doubling and spin–orbit splitting (both, however, are considered in the term energies), however, this does not significantly impact on our spectroscopic simulation outcome as also shown by Luque *et al* [7] in their spectral simulation of OH LIF spectra.

Finally, the energy terms and matrix elements for the two-photon transitions via the 53 different intermediate states ($0 \le v \le 10$ for X state and $0 \le v \le 8$ for A state) were accounted for in the current simulation. Note that we ignore the bounded high-lying $B^2\Sigma^+$ and $C^2\Sigma^+$ excited states of OH and assume that they make no contribution to the two-photon absorption rate since their internuclear equilibrium distances are about twice those of A and X [9].

Cross section and intermediate states of entangled-photon OH absorption. — We now demonstrate the unique and remarkable behavior of the entangled-photon absorption cross section of OH based on the theory and the molecular database described above. In the theoretical implementation of this technique, we follow the basic procedure described by Saleh *et al* [2]. For our simulations, we assume a monochromatic pump with the frequency $\omega_p = \varepsilon_f - \varepsilon_i$ (= 32,605.94 cm^{-1} or 306.77 nm) and parallel-polarized entangled photons with $A_e = 10^{-6}$ cm^2 [1,2]. The final-state linewidth function is assumed to be Lorentzian and the final-state radiative lifetime derived from the spontaneous emission coefficient is 711.6 ns [7].

Figure 3a shows the *non-monotonic* variation of the entangled two-photon absorption cross section of OH as a function of the entanglement time T_e, for the degenerate two-photon case. In this Figure, we also show the *monotonic* behavior of the classical two-

photon absorption cross section. In contrast with the classical absorption, a cyclic oscillation of the entangled-photon cross section σ_e is clearly visible with large variations that arise from the exponential term containing T_e in Eq. (2). The fact that the variations in σ_e can exceed two orders of magnitude (for $T_e < \sim 50$ fs) requires a T_e tuning technique with femto-second precision to achieve the highest level of absorption. From Fig. 3a, we can also see the nonlinear variation in the depth of σ_e (inset right above in Fig. 3a) – this is because the curve is a summation of the trigonometric (exponential) functions with a wide range of frequency difference depending on Δ_j^k. The non-degenerate absorption rate of OH is shown in Fig. 3b. The behavior of the non-degenerate σ_e is highly nonmonotonic and unpredictable (without a theoretical simulation) compared with the degenerate case. The overall frequency of the oscillations in σ_e decreases with increasing pump photon energy difference. It is worthy to note that a real case absorption cross section would likely be ensemble of degenerate and non-degenerate σ_e over a range of pump degeneracy since the SPDC spectrum is broad band, and it is not practical to use a narrow-band (<0.5 nm) interference filter to approximate a monochromatic pump source.

The Fourier transform of the weighted-and-averaged entangled-photon absorption cross section of OH calculated from Eq. (4) is shown in Fig. 4. In order to obtain such a high-quality Fourier spectrum that is able to show very small peaks in Fig. 4a, appropriate T_e and τ_e tunings are required over a certain range with a certain resolution. A reasonable range of the entanglement-time integration is found to be 20 ps for the current molecular system after considering the largest value of $1/|\varepsilon_j - \varepsilon_k|$ (= 5.3 ps) with a multiplication factor of ~4X. A minimum value of the entanglement time $T_e^{\min}$ (or starting value of T_e tuning), which is equivalent to the maximum range of the relative-

path-delay $\tau_e^{\max}$, is estimated to be 67 ps when we apply the relationship that the best possible spectral resolution is governed by the inverse of $T_e^{\min}$ [2]. We seek a 0.5 cm^{-1} spectral resolution for Fourier analysis (i.e. $1/T_e^{\min} \approx 0.5$ cm^{-1}). The spectral range of the Fourier transform $\tilde{\omega}_F$ is determined by the sampling number N_s over the range of τ_e from 0 to $\tau_e^{\max}$, i.e. $\tilde{\omega}_F \geq N_s/2\tau_e^{\max}$. By considering a spectral range required to cover the possible large energy mismatches as $\varepsilon_f - \varepsilon_i - \omega_p/2 = 16{,}303$ cm^{-1}, a reasonable N_s is found to be 2^{16}, thus a τ_e tuning increment is $\tau_e^{\max}/N_s = \sim 1.0$ fs.

To demonstrate the dependence of the absorption cross section Fourier spectrum on the τ_e tuning *range*, two spectra are calculated for the same molecular system but with short (3 ps) and wide (45 ps) ranges of τ_e at the same sampling number N_s. As clearly shown in Fig. 5, a wider range of the relative-path-delay tuning brings a higher resolution for detection of peaks, thus energy levels.

From the above parametric analysis of the entanglement tuning aspects, we found that a 10 to 100 ps range is required for tuning the entanglement time T_e, and about 1 fs resolution for the tuning increment are required in order to obtain a high-resolution (0.5 cm^{-1}) energy spectrum of the OH *A–X* system.

The virtual-state spectroscopy of OH is explicitly realized in Fig. 4, which shows nine distinct observable peaks over three different regions of Δ_j with various amplitudes. Each peak is assigned to one of the intermediate states involved in the transition. From Eq. (3) for the degenerate pump case ($\omega_k^0 = \omega_p/2$), the intermediate state energy is given by $\varepsilon_j = \pm\Delta_j + (\varepsilon_i + \omega_p/2)$. We then need a priori knowledge of the molecule's lowest

intermediate state energy level [2], which is 768.36 cm^{-1} for the current system, and whose energy mismatch $|\Delta_j|$ (16078.82 cm^{-1}) is marked by an arrow in Fig. 4b. In order to identify the corresponding intermediate states from the peak location, we use the relation $\varepsilon_j = +\Delta_j + (\varepsilon_i + \omega_p/2)$, which should be applied to peaks whose $|\Delta_j|$ value is larger than that of the lowest intermediate state. Since the amplitude of the Fourier transform is proportional to $|A_j|^2$, only intermediate states whose transition matrix elements (or transition probability) D_j are relatively large appear in the spectrum. By reading frequencies of the peaks in Fig. 4b we are able to identify four major intermediate states (labeled as v ~ viii) which make a significant contribution to the absorption cross section. It is found that these major intermediate states are not those that lie midway between $v'' = 0$ and $v' = 0$ (such as $v'' = 5$ level of $X^2\Pi_i$), but they are the low-lying levels ($v = 0$) in $X^2\Pi_i$ and $A^2\Sigma$. Hence, this technique is capable of identifying the exact two-photon paths that are dominant for the rovibronic transition. Furthermore, a remarkable observation is that an entanglement-induced two-photon molecular excitation from $|\psi_{v''J''}\rangle$ to $|\psi_{v'J'}\rangle$ of OH can occur through a virtual state whose energy eigenvalue is *larger* than the incident pump energy (32,605.94 cm^{-1}) as evident in Fig. 4c. Here, the frequency peak at Δ_j = 6,068 cm^{-1} is interpreted as $A^2\Sigma$ ($v = 1$, $N = 5$), whose energy is 35,911.73 cm^{-1}. Note that this *apparent* violation of energy conservation can be explained because of the fact that this phenomenon arises from a coherent summation of the two-photon terms through the effects of fourth-order quantum coherence [2], which allows a virtual-state transition-path-scan to be performed in entanglement *time*-space. Specifically, if we examine Eqs. (4) and (5), we see that there is no limitation for the values of the energy

mismatch Δ_j, while the energy conservation for the initial-to-final transition is implicitly ensured by the δ-function in Eq. (4). Thus, the conservation of energy is not actually violated. This unusual but distinct result follows a similar observation by Saleh *et al* [2] for atomic hydrogen.

In the present non-classical technique, the virtual-states of the OH molecule in the A-X system are observable through a transition-path-scan which reveals individual intermediate-state information; such information is impossible to obtain using a classical two-photon spectroscopy [9]. While there are challenges to an experimental realization of this technique, the experimental implementation in principle is achievable if certain experimental parameters described above are satisfied. The new and unique features of entangled biphoton virtual-state spectroscopy as applied to OH demonstrate that this technique may be useful for spectroscopically probing difficult-to-access states of other molecular systems.

The authors acknowledge Dr. Jorge Luque, Lam Research Corporation, CA, USA for providing variable information on molecular database of OH. This research was supported by the Ultra-Efficient Engine Technologies (UEET) Program at NASA Glenn Research Center. The work was performed while J. K. held a National Research Council Research Associateship Award at NASA GRC.

References

1. H.-B. Fei, B. M. Jost, S. P. Popescu, B. E. A. Saleh, and M. C. Teich, "Entanglement-induced two-photon transparency," Phys. Rev. Lett. 78 (1997) 1679-1682.
2. B. E. A. Saleh, B. M. Jost, H.-B. Fei, and M. C. Teich, "Entangled-photon virtual-state spectroscopy," Phys. Rev. Lett. 80 (1998) 3483-3486.

3. J. Peřina, Jr., B. E. A. Saleh, and M. C. Teich, "Multiplephoton absorption cross section and virtual-state spectroscopy for the entangled n-photon state," Phys. Rev. A 57 (1998) 3972-3986.

4. M. C. Teich, and B. E. A. Saleh, "Entangled-photon microscopy, spectroscopy, and display," U.S. Patent No. 5,796,477 (Aug. 1998).

5. M. C. Teich, and G. J. Wolga, "Multiple-photon process and higher order correlation functions," Phys. Rev. Lett. 16 (1966) 625-628.

6. L. S. Rothman, C. P. Rinsland, A. Goldman, S. T. Massie, D. P. Edwards, J.-M. Flaud, A. Perrin, C. Camy-Peyret, V. Dana, J.-Y. Mandin, J. Schroeder, A. McCann, R. R. Gamache, R. B. Wattson, K. Yoshino, K. V. Chance, K.W. Jucks, L.R. Brown, V. Nemtchinov, and P. Varanasi, "The HITRAN Molecular Spectroscopic Database and HAWKS (HITRAN Atmospheric Workstation): 1996 Edition," J. Quant. Spectrosc. Radiat. Transfer 60, 665-710 (1998).

7. J. Luque and D.R. Crosley, "LIFBASE: Database and spectral simulation (version 1.5)", SRI International Report MP 99-009 (1999).

8. K. C. Smith, and D. R. Crosley, "Chapter 2: Detection of minor species with laser techniques," Applied Combustion Diagnostics (ed. K. Kohse-Hoinghaus and J. B. Jeffries), Taylor & Francis, London, 9-68.

9. D. R. Crosley, and G. P. Smith, "Two-photon spectroscopy of the $A^2\Sigma^+$–$X\ ^2\Pi$i system of OH," J. Chem. Phys. 79 (1983) 4764-4773.

10. J. E. M. Goldsmith, and N. M. Laurendeau, "Two-photon-excited fluorescence measurements of OH concentration in a hydrogen-oxygen flame," Appl. Opt. 25 (1986) 276-283.

11. Q.-V. Nguyen, and P. H. Paul, "Photochemical effects of KrF Excimer excitation in laser-induced fluorescence measurements of OH in combustion environments," Appl. Phys. B 72 (2001) 497-505.

12. A. V. Sergienko, Y. H. Shin, and M. H. Rubin, "Experimental evaluation of a two-photon wave packet in type-II parametric downconversion," J. Opt. Soc.Am. B 12 (1995) 859-862.

13. A. Joobeur, B. E. A. Saleh, T. S. LArchuk, M. C. Teich, "Coherence properties of entangled light beams generated by parametric down-conversion: theory and experiment," Phys. Rev. A 53 (1996) 4360-4371.

14. A. Joobeur, B. E. A. Saleh, and M. C. Teich, "Spatiotemporal coherence properties of entangled light beams generated by parametric down-conversion," Phys. Rev. A 50 (1994) 3349-3361.

15. R. P. Cageao, Y. L. Ha, Y. Jiang, M. F. Morgan, Y. L. Yung, and S. P. Sander, "Calculated hydroxyl $A^2\Sigma$–$X\ ^2\Pi$ (0,0) band emission rate factors applicable to atmospheric Spectroscopy," J. Quant. Spectrosc. Radiat. Transfer 57 (1997) 703-717.

16. G. H. Dieke, and H. M. Crosswhite, "The ultraviolet bans of OH: fundamental data," J. Quant. Spectrosc. Radiat. Transfer 2 (1962) 97-199.

17. J. Luque and D. R. Crosley, "Transition probabilities in the $A^2\Sigma^+$–$X\ ^2\Pi_i$ electronic system of OH," J. Chem. Phys. 109 (1998) 439-448.

18. R. R. Gamache, and L. S. Rothman, "Extension of the HITRAN database to non-LTE application," J. Quant. Spectrosc. Radiat. Transfer 48 (1992) 519-525.

19. R. J. Le Roy, "LEVEL 7.5: a computer program for solving the radial Schrodinger equation for bound and quasibound levels," University of Waterloo Chemical Physics Research Report CP-655 (2002).

20. R. J. Le Roy, "RKR1 2.0: a computer program implementing the first-order RKR method for determing diatomic molecule potential energy functions," University of Waterloo Chemical Physics Research Report CP-657 (2003).

21. D. Hirst, A computational approach to chemistry, Blackwell Scientific, London, (1990) 124-130.

Figure Captions

Fig. 1 The potential energy curves for the electronic ground (X) and excited (A) states of OH calculated using the RKR method, showing a model of a two-photon absorption transition $\varepsilon_i \rightarrow \varepsilon_f$ via an intermediate (virtual) state ε_j and the energy mismatch Δ_j.

Fig. 2 Schematic diagram of the selection-rule allowed two-photon OH rovibronic transitions for the $R_1(5)$ X–A absorption. The Λ-splitting is omitted here.

Fig. 3 Entangled two-photon absorption cross sections for $R_1(5)$ transition in molecular OH A–X system over a range of the entanglement time. (a) Degenerate pump. *Solid line*: with nonclassical (entangled) light source. *Dashed line*: with classical light source. (b) Non-degenerate pump. *Solid line*: photon-pair frequency ratio is 1:3. *Dashed line*: photon-pair frequency ratio is 1:7.

Fig. 4 Energy spectrum obtained by taking the Fourier transform of the averaged absorption cross section for the entangled two-photon OH A–X $R_1(5)$ transition as a function of the energy mismatch for an entanglement-time integration range $67 < T_e \leq 87$ ps and a relative-path-delay tuning range $0 \leq \tau_e \leq 67$ ps with a tuning increment $\delta\tau_e = 1.0$ fs. The peaks are labeled by f_1, f_2, and F for $X^2\Pi_{3/2}$, $X^2\Pi_{1/2}$, and $A^2\Sigma$ state, respectively with (v, N) notation.

Fig. 5 Dependence of the energy spectrum on the tuning range of τ_e for the same molecular transition in Fig. 5. *Solid line*: $45 < T_e \leq 65$ ps, $0 \leq \tau_e \leq 45$ ps, $\delta\tau_e = 2.7$ fs. *Dashed line*: $3 < T_e \leq 23$ ps, $0 \leq \tau_e \leq 3$ ps, $\delta\tau_e = 0.18$ fs. Refer Fig. 4 for the labels.

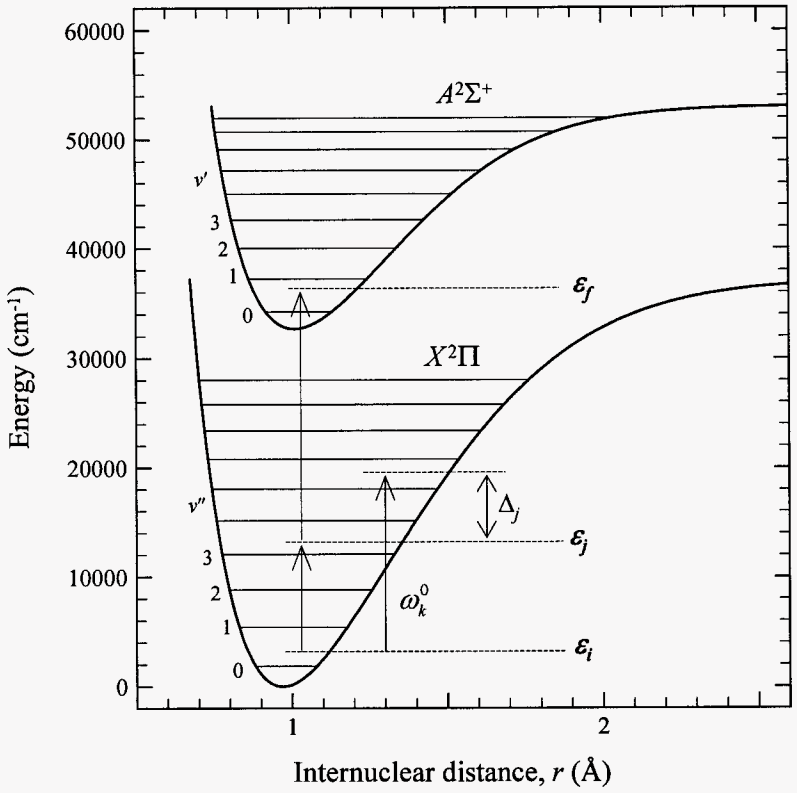

Fig. 1 The potential energy curves for the electronic ground (X) and excited (A) states of OH calculated using the RKR method, showing a model of a two-photon absorption transition $\varepsilon_i \rightarrow \varepsilon_f$ via an intermediate (virtual) state ε_j and the energy mismatch Δ_j.

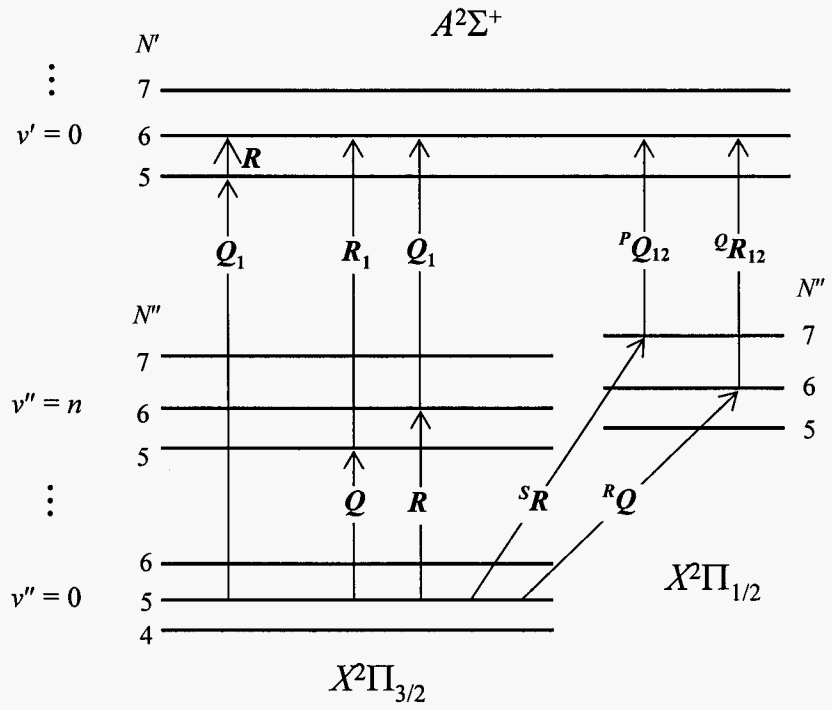

Fig. 2 Schematic diagram of the selection-rule allowed two-photon OH rovibronic transitions for the $R_1(5)$ X–A absorption. The Λ-splitting is omitted here.

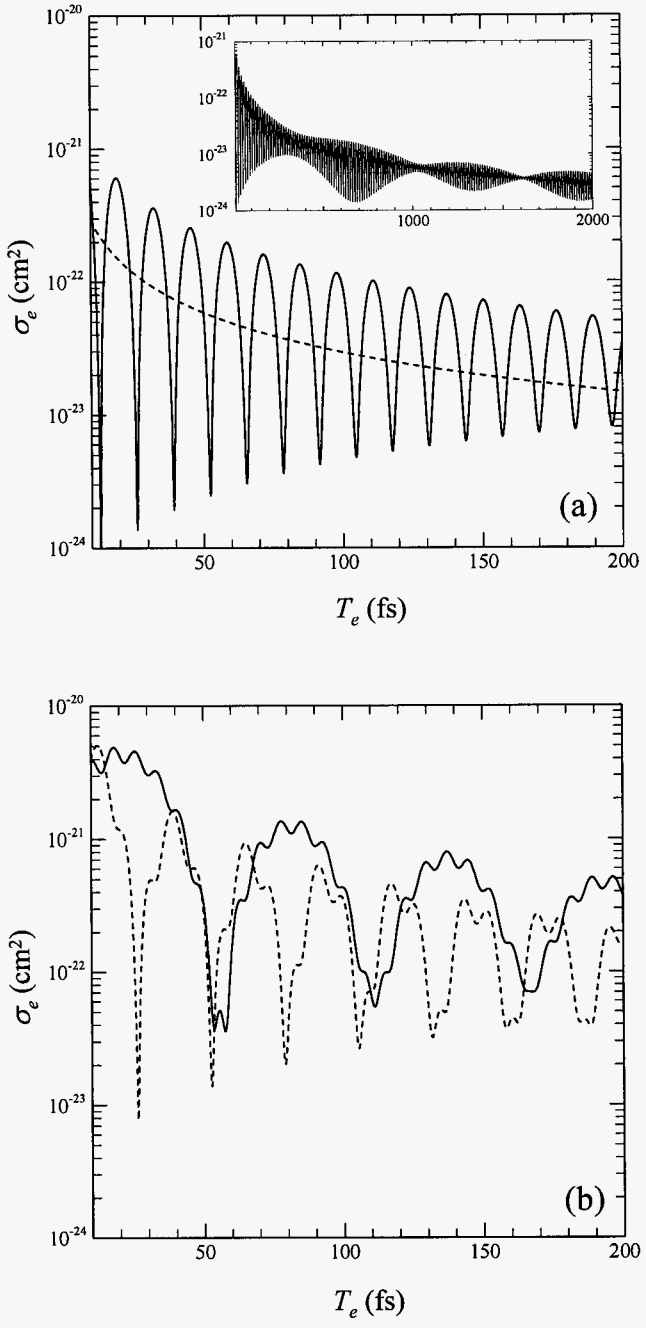

Fig. 3 Entangled two-photon absorption cross sections for $R_1(5)$ transition in molecular OH A–X system over a range of the entanglement time. (a) Degenerate pump. *Solid line*: with nonclassical (entangled) light source. *Dashed line*: with classical light source. (b) Non-degenerate pump. *Solid line*: photon-pair frequency ratio is 1:3. *Dashed line*: photon-pair frequency ratio is 1:7.

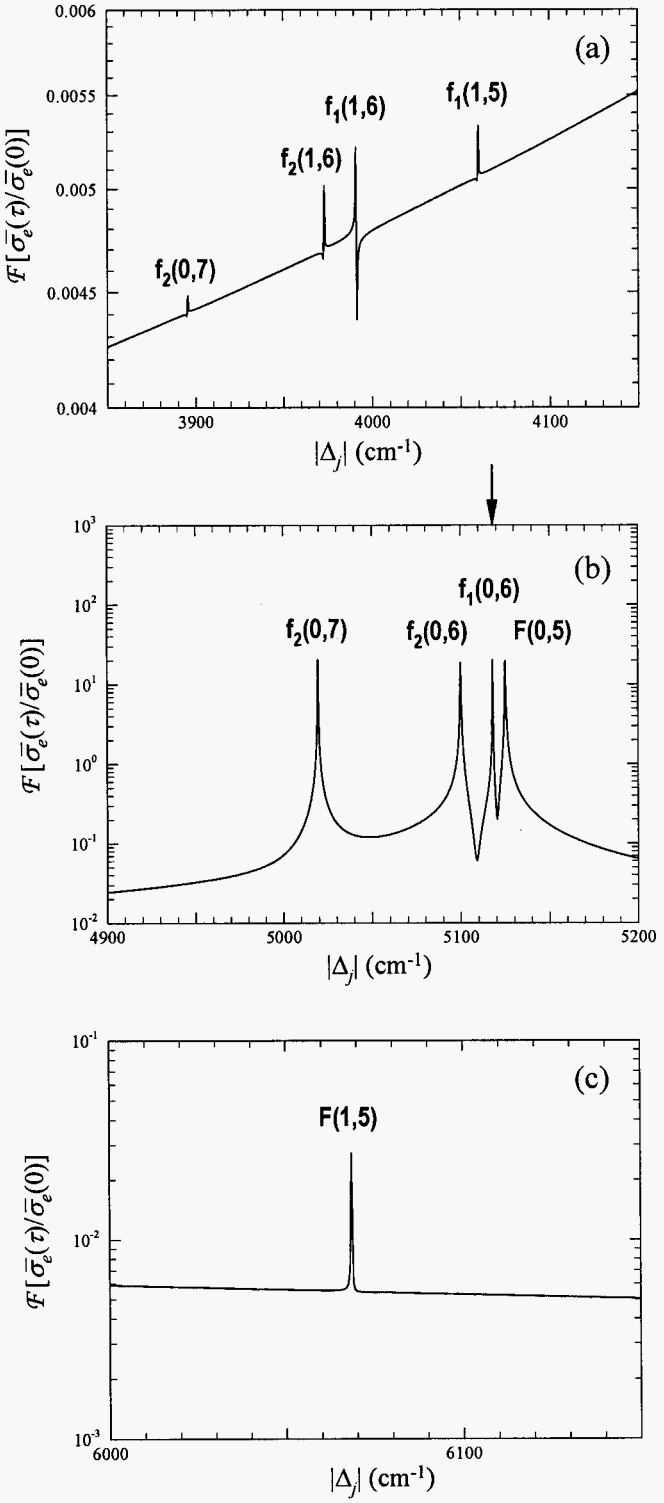

Fig. 4 Energy spectrum obtained by taking the Fourier transform of the averaged absorption cross section for the entangled two-photon OH A–X $R_1(5)$ transition as a function of the energy mismatch for an entanglement-time integration range $67 < T_e \leq 87$ ps and a relative-path-delay tuning range $0 \leq \tau_e \leq 67$ ps with a tuning increment $\delta\tau_e = 1.0$ fs. The peaks are labeled by f_1, f_2, and F for $X^2\Pi_{3/2}$, $X^2\Pi_{1/2}$, and $A^2\Sigma$ state, respectively with (v, N) notation.

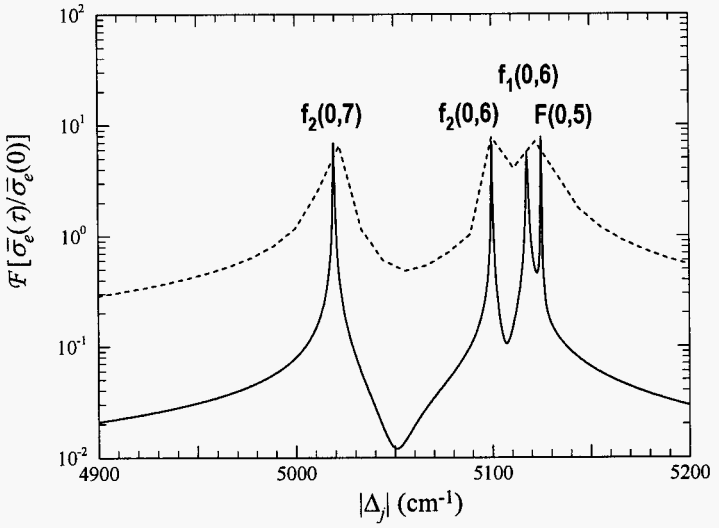

Fig. 5 Dependence of the energy spectrum on the tuning range of τ_e for the same molecular transition in Fig. 5. *Solid line*: $45 < T_e \leq 65$ ps, $0 \leq \tau_e \leq 45$ ps, $\delta\tau_e = 2.7$ fs. *Dashed line*: $3 < T_e \leq 23$ ps, $0 \leq \tau_e \leq 3$ ps, $\delta\tau_e = 0.18$ fs. Refer to Fig. 4 for the labels.